Supplementary Information (SI) for Biomaterials Science.
This journal is © The Royal Society of Chemistry 2026

Supporting Information of

A Spatiotemporally Controllable Magnetic Microneedle for Targeted Gastric Drug Delivery

Jun Luo [a, ‡], Shuyue Deng [a, ‡], Shibo Zhang [a], Yanbing Zhao [a], Xinyi Xu [b], Ran An [b], Jianjun Dai [a, b, *], Yanmin Ju [a, *]

[a]College of Pharmacy, China Pharmaceutical University, Nanjing 211198, China

[b]MOE Joint International Research Laboratory of Animal Health and Food Safety, Key Laboratory of Animal Bacteriology, Ministry of Agriculture, College of Veterinary Medicine, Nanjing Agricultural University, Nanjing 210095, China

*Corresponding authors E-mail: jjdai@cpu.edu.cn (Jianjun Dai), juyanmin@cpu.edu.cn (Yanmin Ju).

‡ These authors contributed equally to this study as co-first authors

SUPPORTING EXPERIMENTAL SECTION

Drug loading capacity. R-B loading quantified via UV-Vis at 554 nm. MTZ and PTX content were analyzed by HPLC. CLA was quantified through chromogenic oxidation by strong acids, followed by UV-Vis detection at 482 nm. Insulin loading was determined using a BCA assay.

Morphology characterization of SMM. The morphology of the containers and intact SMM was recorded by digital microscope (XTL-500, Jifei, China), scanning electron microscope (SU5000, HITACHI, Japan). The height of the micro-cavity in containers was calibrated and recorded. Fluorescein mages of the SMM were then recorded by confocal laser scanning microscope (STELLARIS 8 Confocal, Leica, Germany).

Drug release behavior of SMM in vitro. SMMs loaded with paclitaxel, metronidazole and insulin were separately placed in 10 mL PBS (pH = 7.4) and shaken at 200 rpm at 37℃. 1 mL of release medium was taken to test at predetermined time intervals as sample solution (0, 2, 4, 6, 10, 20, 40, and 60 min) and replenished with the same volume of fresh release medium. The sample solution of paclitaxel and metronidazole were then assayed by HPLC-UV after filtrating. HPLC-UV experimental conditions: reversed-phase C_{18} column (250 mm by 4.6 mm, inner diameter, 5 μm particle size). Methyl alcohol and distilled water (7:3 ratio, v/v) formed the mobile phase. The injection volume was 20 μL, with a flow temperature of 37°C and a flow rate of 1 mL min^{-1}. The sample solution of insulin was assayed by BCA Protein Assay Kit. The amount of paclitaxel, metronidazole and insulin released from SMM was calculated and the cumulative release curve was plotted. To determine the release kinetics of paclitaxel and metronidazole, the release data were plotted on following four kinetic models, including first-

order model, zero-order model, Higuchi model and Korsmeyer-Peppas model[1]. The model that fit best was used to represent the pattern of paclitaxel and metronidazole released from MNPs. The mathematical equations for release kinetic model:

Zero-order model:

$$M_t = K \times t \tag{1}$$

First-order model:

$$\ln\left(1 - M_t\right) = - K \times t \tag{2}$$

Higuchi model:

$$M_t = K \times t^{0.5} \tag{3}$$

Korsmeyer-Peppas model:

$$M_t = K \times t^n \tag{4}$$

Where M_t represents the cumulative percentage of drug released in time, K is the rate constant and n is drug release exponent.

Mechanical tests of SMM. Mechanical compression tests of the SMM were performed using a force test bench (TH-8203S, Tophung, China). Briefly, One SMM was placed in the center of the rigid stainless-steel platform (with the tips of the containers facing upward). The test station sensor probe moved toward the SMM at a speed of 0.1 mm s^{-1}. Force and displacement measurements began when the transducer first touched the tips of containers and continued until the force applied to the transducer from the containers reached 70 N and stopped. The mechanical strength of the SMM prepared with different concentrations of HP-50 and R-B

powders was tested firstly. Then the mechanical strength of the SMM prepared with 1% HP-50 and different drug powders was further tested.

Antibacterial test of SMM. *Helicobacter pylori* (*H. pylori*) ATCC 26695 was used to test the antimicrobial properties of SMM. The bacteria were cultured on Columbia blood plates supplemented with fetal bovine serum (FBS, 200 μL) for 3-4 days at 37°C under microaerophilic conditions. Then, the bacterial were harvested and resuspended in brain heart infusion liquid medium with 10% FBS. Bacterial growth was measured by reading optical density at 600 nm (OD600). For a typical antibacterial test, *H. pylori* were cultured with clarithromycin (CLA) and clarithromycin-loaded SMM (SMM-C), respectively, receiving equivalent CLA doses at 10 μg mL^{-1}. After incubation at 37℃ under microaerobic conditions for 16 hours, the OD600 was tested and then circulated the antibacterial rate. For a disk diffusion test, *H. pylori* (OD600 = 1.0) were spread with a cotton swab in the Columbia blood plate and waited for dry. Then three disks (CLA, SMM-C, Control) were added on the plate. After incubation at 37℃ under microaerobic conditions for 16 hours, the inhibit zones were measured by the dial caliper.

Magnetic performance of SMM. The SMM was magnetized with an output voltage of 600 V for two times to achieve uniform axial magnetization, using a pulsed magnetizer (J302, Jinlang Co. Ltd., Nanjing, China). A cylindrical magnet (30 mm in diameter and 30 mm in height, 4000 GS) provided external magnetic actuation[2]. SMM prototypes were fabricated with varying NdFeB concentrations (10-30% w/v) in the PCL matrix. The magnetic hysteresis loop of SMM prototypes were measured using a vibrating sample magnetometer (Model 3100, East Changing, China). The SMM prototypes were fixed on the sample holder. All measurements were

performed at room temperature (300 K) with an applied magnetic field sweeping between -20 kOe and +20 kOe. The raw magnetic moment data were corrected for the diamagnetic contribution of the sample holder and normalized by the sample mass to obtain the mass magnetization (emu/g). The maximum response distance (magnet-to-SMM) was then measured to optimize NdFeB loading. The magnetic controllability of SMM was validated through programmed magnetic navigation, achieving precise trajectory tracking (C/P/U/D/J patterns) through combined tumbling and translational motions. Human palm served as an anatomical proxy for *in vivo* conditions. Counter-rotation was achieved by opposite-phase magnet rotation beneath the palm. In order to simulate the real spatial interaction and viscoelastic gastric mucosa, a 3D-printed stomach model lined with 1% agarose gel was employed. The anti-gravity climbing of SMM along the lesser curvature was recorded (iPhone 14, Apple, USA).

Penetration and retention behavior of SMM in vitro. The penetration capability of SMMs was evaluated through following approaches. 1% agarose hydrogel was prepared to mimic a wet and soft stomach mucus layer [3]. Firstly, the force to penetrate the agarose hydrogel and attract with the magnet was tested using a tensiometer (TH-8203S, Suzhou Tophung Machine Equipment Co., Ltd., Suzhou, China). Secondly, the SMM was placed on 1% agarose hydrogel and subjected magnetic force of the magnet for 10 minutes. Following removal of both magnet and SMM, penetration channels in the hydrogel were imaged. Freshly isolated rabbit gastric mucosa was employed for ex vivo penetration validation. Identical magnetic actuation protocols were applied, and resultant mucosal penetration tracks were documented. Tissue sections containing penetration sites were processed for histological evaluation.

The retention capability was evaluated using a custom flow chamber apparatus adapted from previous work[3]. 1% (w/v) agarose solution was cast into the chamber and allowed to gel at room temperature for 30 min. The SMM was positioned on the gel surface with a NdFeB magnet placed 2 cm beneath the chamber. The chamber was inclined at 45° and flushed with water at 99 mL min^{-1}. The SMM displacement was tracked. Another SMM without magnetic application served as the negative control under identical flow conditions.

The mucosal-responsive disintegration of containers in SMF and SGF. Simulated gastric fluid (SGF, pH = 3) and simulated mucus fluid (SMF, pH = 7) was prepared by following method [4]. SGF was consist of 6.9 mmol L^{-1} KCl, 0.9 mmol L^{-1} KH_2PO_4, 25 mmol L^{-1} $NaHCO_3$, 47.2 mmol L^{-1} NaCl, 0.1 mmol L^{-1} $MgCl_2(H_2O)_6$, 0.5 mmol L^{-1} $(NH_4)_2CO_3$ and 15.6 mmol L^{-1} HCl. Using simulated intestinal fluid as SMF, which consisted of 6.8 mmol L^{-1} KCl, 0.8 mmol L^{-1} KH_2PO_4, 85 mmol L^{-1} $NaHCO_3$, 38.4 mmol L^{-1} NaCl, 0.33 mmol L^{-1} $MgCl_2(H_2O)_6$ and 8.4 mmol L^{-1} HCl.

The muco-responsive disintegration process was monitored through fluorescent tracer release with some modification[5]. The SMMs with C-6 labeled containers were incubated in SMF and SGF at 37℃, respectively. The disintegration level of SMMs was recorded at predetermined time intervals (0, 2, 4, and 8 min) by optimal microscope. SMMs loaded with R-B were incubated in SMF and SGF at 37℃, respectively. The fluorescence changes were observed at predetermined time intervals (0, 2, 6, 10, and 20 min) and the fluorescence intensity was analyzed in ImageJ (Version 2020).

Analysis of ZO-1 protein expression. GES-1 cells were lysed in RIPA buffer with protease inhibitors. Protein concentration was measured by BCA assay. Equal amounts of protein were separated by 8% SDS-PAGE and transferred onto PVDF membranes. Membranes were blocked with 5% non-fat milk in TBST for 1 h, then incubated with anti-ZO-1 antibody (1:1000, Cell Signaling) overnight at 4°C. After washing, membranes were incubated with HRP-conjugated secondary antibody (1:5000) for 1 h. Protein bands were detected using ECL substrate. GAPDH was used as a loading control.

Stability of the base in different medium. The base was recorded of initial weight, then incubating in different medium at 37℃ with gentle stirring[2]. At a predetermined time, the base was picked up and dried. Then the dry weight was recorded. The ratio of the dry weight to the initial weight was the relative weight change of the base.

Cytotoxicity assay of the base. The base and pure NdFeB powders were incubated in SGF at 37℃ with gentle stirring. At 2, 4, and 6-hour intervals, 1 mL leaching solution was aseptically collected, centrifuged and filter-sterilized for cytotoxicity testing. GES-1 cells were seeded in 96-well plates and cultured to reach 80% confluency, then incubating with leaching solution for 24 h. 20 μL MTT reagent was added to each well and incubated for 4 h.

Immunogenicity of SMM. The blank SMMs without any loading were incubated with GES-1 cells at 37℃. Untreated GES-1 cells served as the control group. Total RNA was extracted using Trizol, and then reverse-transcribed into cDNA. Next, qPCR was performed to quantify the gene expression levels of IL-6 and TNF-α.

Blood compatibility of SMM. Blood from healthy New Zealand rabbit was utilized to evaluate the hemocompatibility of SMM. Specifically, 50 μL of 2% red blood cell suspension was mixed with different concentrations of SMM and incubated at 37°C for 3 h. The positive and negative control groups were pure water and PBS (pH = 7.4), respectively. Finally, the absorbance of supernatant was collected at 540 nm. The hemolysis rate was calculated as follows:

$$Hemolysis\ (\%) = (A_S - A_N)/(A_P - A_N) \times 100\% \quad (5)$$

Where A_S represents the absorbance values of supernatant of samples, A_N is the absorbance values of saline and A_P is the absorbance values of pure water.

Chemical element analysis in leaching solutions of the base. The iron leaching profile was characterized by incubating base samples in SGF at 37°C for 24 hours. Leached iron ion was quantified using an Iron Detection Kit (Philoxazine colorimetric method).

Magnetic actuation and penetration performance of SMM in canine models. Dogs were provided by Veterinary Teaching Hospital, Nanjing Agricultural University. The dogs were anaesthetized for endoscopy to visualize the in vivo manipulation of the SMM. The SMM was directly put into stomach using a cannula and then manipulated by a magnet (30 mm in diameter and 30 mm in height). Orientation control of the penetrating tip of SMM was achieved through external magnet positioning above the thoracoabdominal junction. By placing the magnet close to the thoracoabdominal junction, the enhanced local magnetic field enabled the SMM penetrate the gastric mucosa.

Drug delivery and glycemic regulation performance of SMM in rabbit models. The drug delivery performance of the SMM was visualized by fluorescence imaging in rabbit model. New Zealand Rabbits (female, 2-2.5 kg) were purchased from Qinglongshan animal breeding ground (Nanjing, China), and were housed and handled under conventional conditions. The experiments were performed in accordance with the Guidelines for Care and Use of Laboratory Animals of China Pharmaceutical University. All animal experiments were approved by the Animal Ethics Committee of School of Pharmacy, China Pharmaceutical University (IACUC-2023-12-006). The rabbits were anaesthetized by intraperitoneal injection of 3% sodium pentobarbital and then a gavage tube was inserted. Following external magnet fixation at the thoracoabdominal junction, SMMs were fed into the stomach through the gavage tube with 5 mL sterile saline flush. The tube was withdrawn after 1-minute dwell time, while maintaining magnet position for 10 minutes. Control animals received equivalent-dose rhodamine B solution via identical administration route. In vivo fluorescence imaging was conducted at predetermined intervals (0, 5, 30, 60, 180 min). Rabbits were then executed and eviscerated, followed by *ex vivo* organ imaging. Other rabbits were executed and eviscerated to tissue damage analysis by H&E staining.

The glycemic regulation performance of SMM was also evaluated in New Zealand Rabbits diabetes models. After 24-hour fasting with free access to water, diabetes was induced by rapid auricular vein injection of 5% alloxan at the dose of 100 mg kg^{-1} body weight in less than 30 s. Food was provided post-injection to prevent hypoglycemic shock. After 14-day stabilization, rabbits with sustained hyperglycemia above 13.9 mM were enrolled[6, 7]. Then, SMMs containing

insulin were delivered into stomach (6 U kg^{-1} body weight) as described above. At predetermined time points, blood glucose was monitored via a glucometer (Sinocare GA-3, Changsha, China). The number of parallel trials for each group was three.

Reference

(1) Deng, S. Y.; Shuai, Y.; Zhang, S. B.; Sun, C. X.; Chang, L.; Xu, J.; Tong, L.; Ji, Q. S.; Li, M.; Dai, J. J., et al.; Personalized demand-responsive biphasic microneedle patch for smart drug administration. *Biomater. Sci.* **2023,** *11* (16), 5605-5617.
(2) Zhang, X. X.; Chen, G. P.; Fu, X.; Wang, Y. T.; Zhao, Y. J.; Magneto-Responsive Microneedle Robots for Intestinal Macromolecule Delivery. *Adv. Mater.* **2021,** *33* (44), No. e2104932.
(3) Chen, W.; Wainer, J.; Ryoo, S. W.; Qi, X. Y.; Chang, R.; Li, J.; Lee, S. H.; Min, S.; Wentworth, A.; Collins, J. E., et al.; Dynamic omnidirectional adhesive microneedle system for oral macromolecular drug delivery. *Sci. Adv.* **2022,** *8* (1), No. eabk1792.
(4) Mulet-Cabero, A. I.; Egger, L.; Portmann, R.; Ménard, O.; Marze, S.; Minekus, M.; Le Feunteun, S.; Sarkar, A.; Grundy, M. M. L.; Carrière, F. C., et al.; A standardised semi-dynamic in vitro digestion method suitable for food - an international consensus. *Food Funct.* **2020,** *11* (2), 1702-1720.
(5) Wu, Y.; Song, Z. Y.; Deng, G. Y.; Jiang, K.; Wang, H. J.; Zhang, X. J.; Han, H. Y.; Gastric Acid Powered Nanomotors Release Antibiotics for In Vivo Treatment of Helicobacter pylori Infection. *Small* **2021,** *17* (11), No. e2006877.
(6) Zhang, X. X.; Chen, G. P.; Cai, L. J.; Fan, L.; Zhao, Y. J.; Dip-Printed Microneedle Motors for Oral Macromolecule Delivery. *Research* **2022,** *2022*, No. 9797482.
(7) Cai, L. J.; Chen, G. P.; Sun, L. Y.; Miao, S. S.; Shang, L. R.; Zhao, Y. J.; Sun, L. Y.; Rocket-Inspired Effervescent Motors for Oral Macromolecule Delivery. *Adv. Mater.* **2023,** *35* (33), No. 2210679.

SUPPORTING Figures

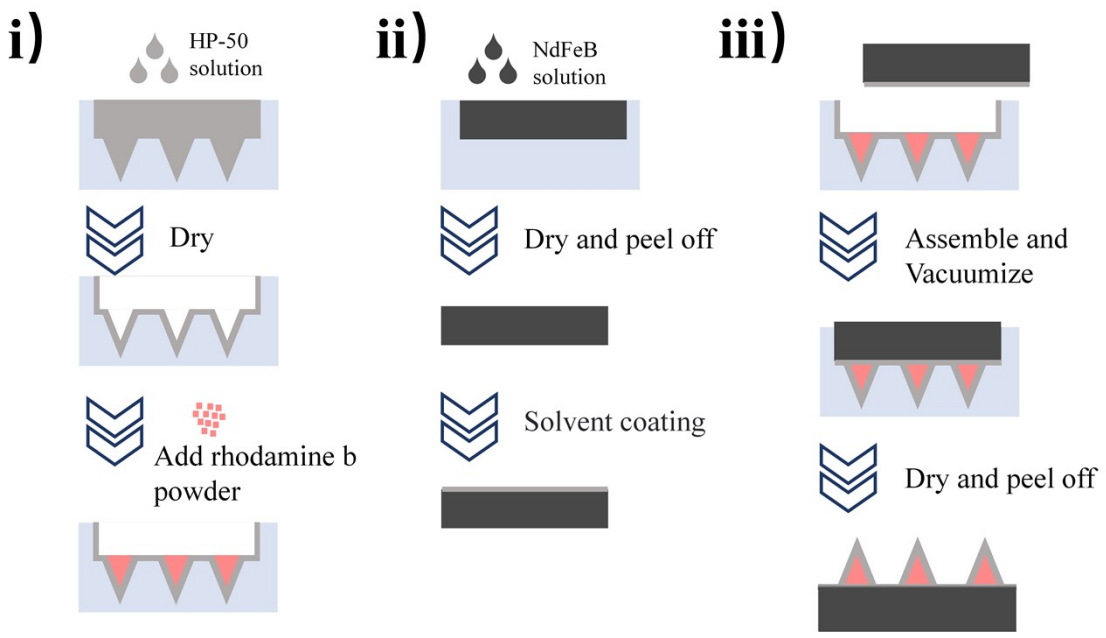

Figure S1. Schematic illustration of the fabrication of SMM. (i) The fabrication process of the container. (ii) The fabrication process of the magnetic base. (iii) The assemble of the container and the magnetic base.

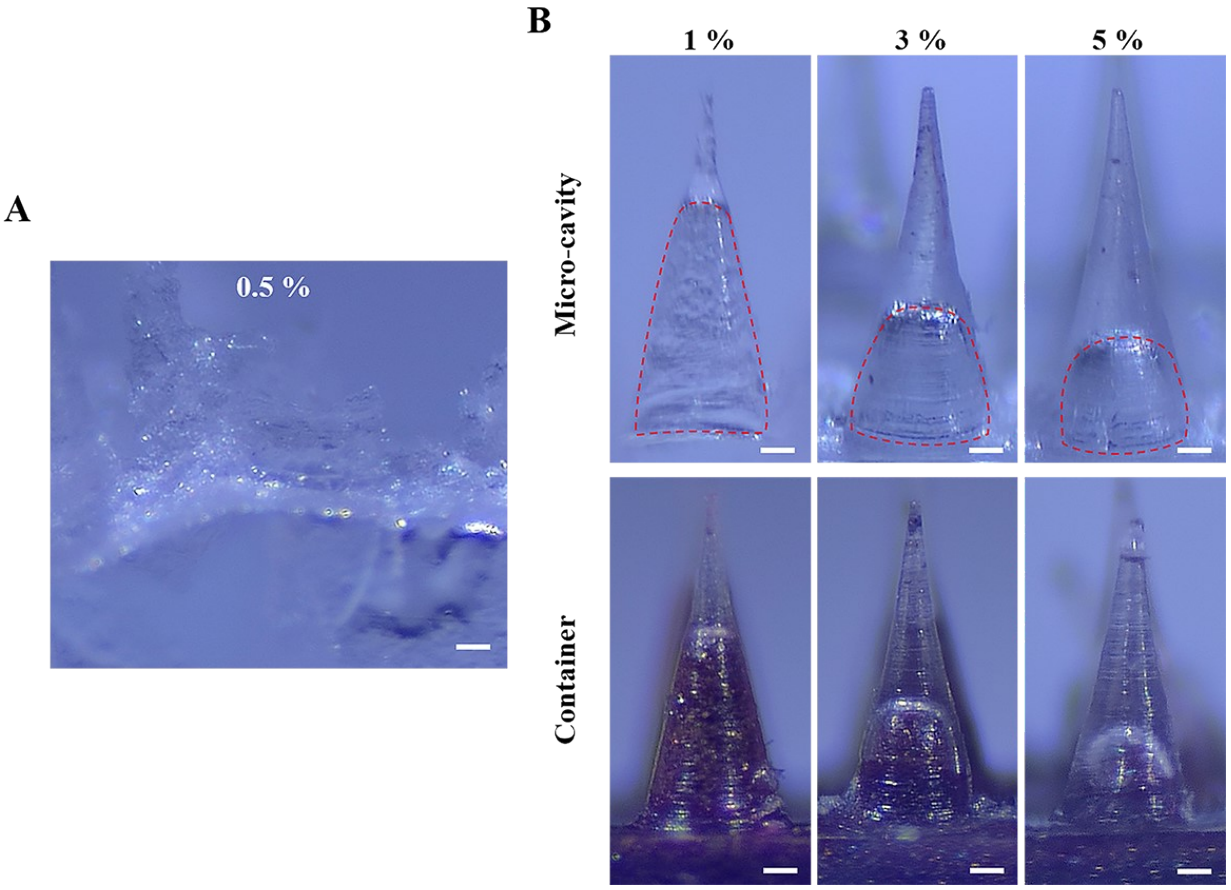

Figure S2. Morphology of the container. (A) Cracked micro-cavity of the container was fabricated with 0.5% HP-50. Scale bar: 100 μm. (B) Tip containers with decreasing micro-cavity volume and rhodamine B powder loading were fabricated with HP-50 concentrations varying from 1% to 5%. Red dotted line dedicated the micro-cavity of the container. Scale bar: 100 μm.

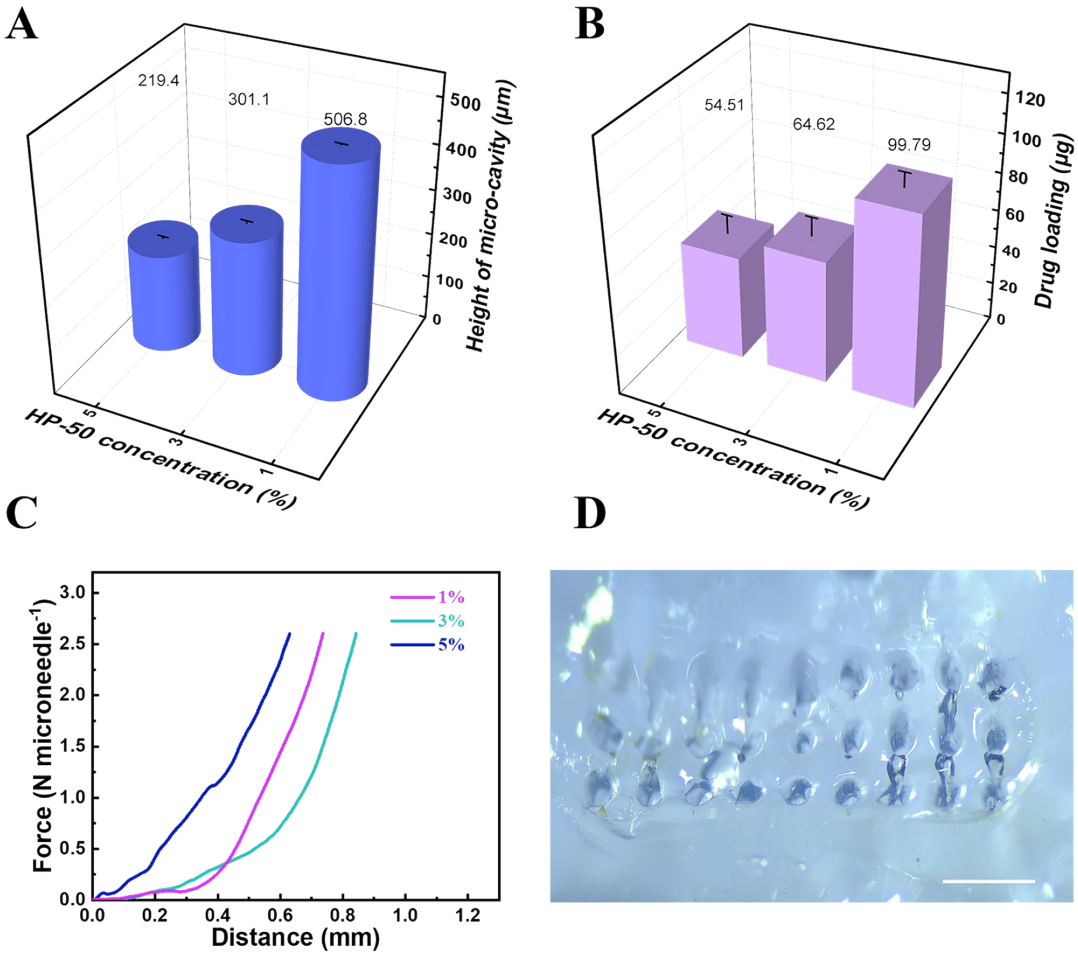

Figure S3. Basic properties of the containers. (A) Quantification of the height of the micro-cavity. The height of the micro-cavity was decreased with the increasing concentration of HP-50. Data were presented as mean ± SD (n = 3). (B) Quantification of the loading capacity of the containers. The drug loading was increased with the decreasing concentration of HP-50. Data were presented as mean ± SD (n = 3). (C) The mechanical forces of the container fabricated with various concentration of HP-50. (D) The photo of penetration traces left in the 1% agarose hydrogel after the administration of SMM made by 1% HP-50. Scale bar: 1000 μm.

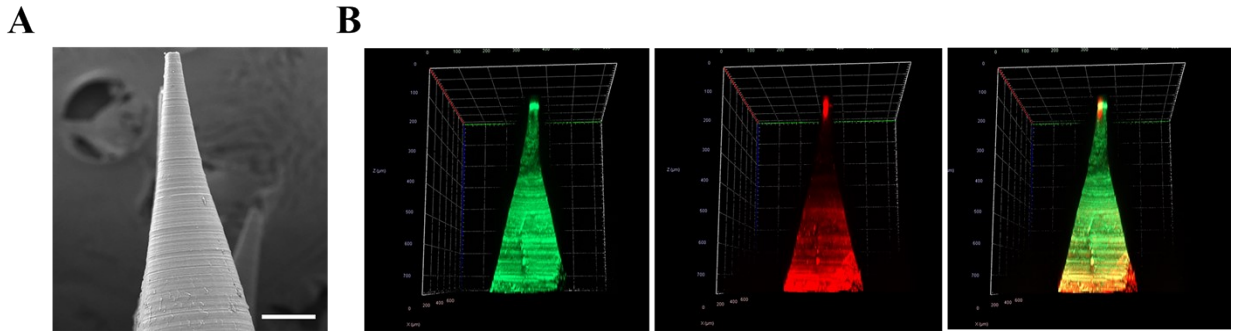

Figure S4. Scanning electron microscope and fluorescence confocal images of SMM. (A) SEM image of SMM. Scale bar: 100 μm. (B) Fluorescence confocal images of various parts of the SMM. Green fluorescence was container added with C-6 and red fluorescence was R-B powder.

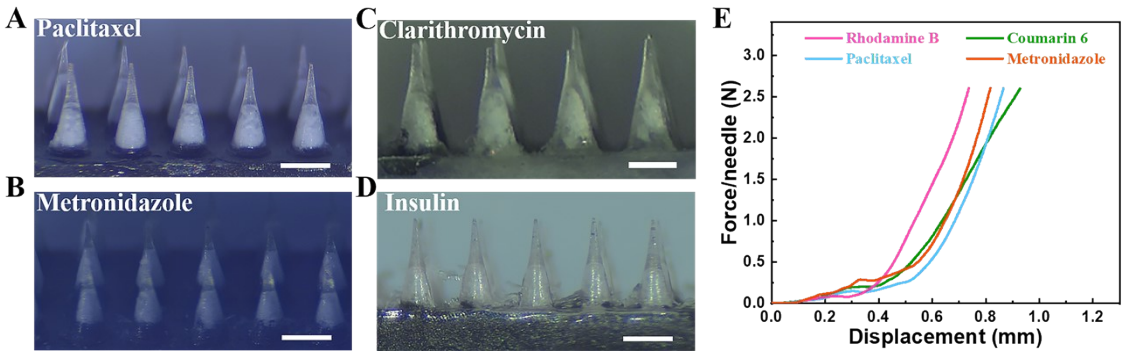

Figure S5. Universal drug-loading capacity and mechanical property of SMM. The morphology of SMM loaded with (A) paclitaxel powder, (B) metronidazole powder, (C) clarithromycin powder, and (D) insulin powder. Scale bar: 500 μm. (E) The mechanical force of SMM loaded with different powders.

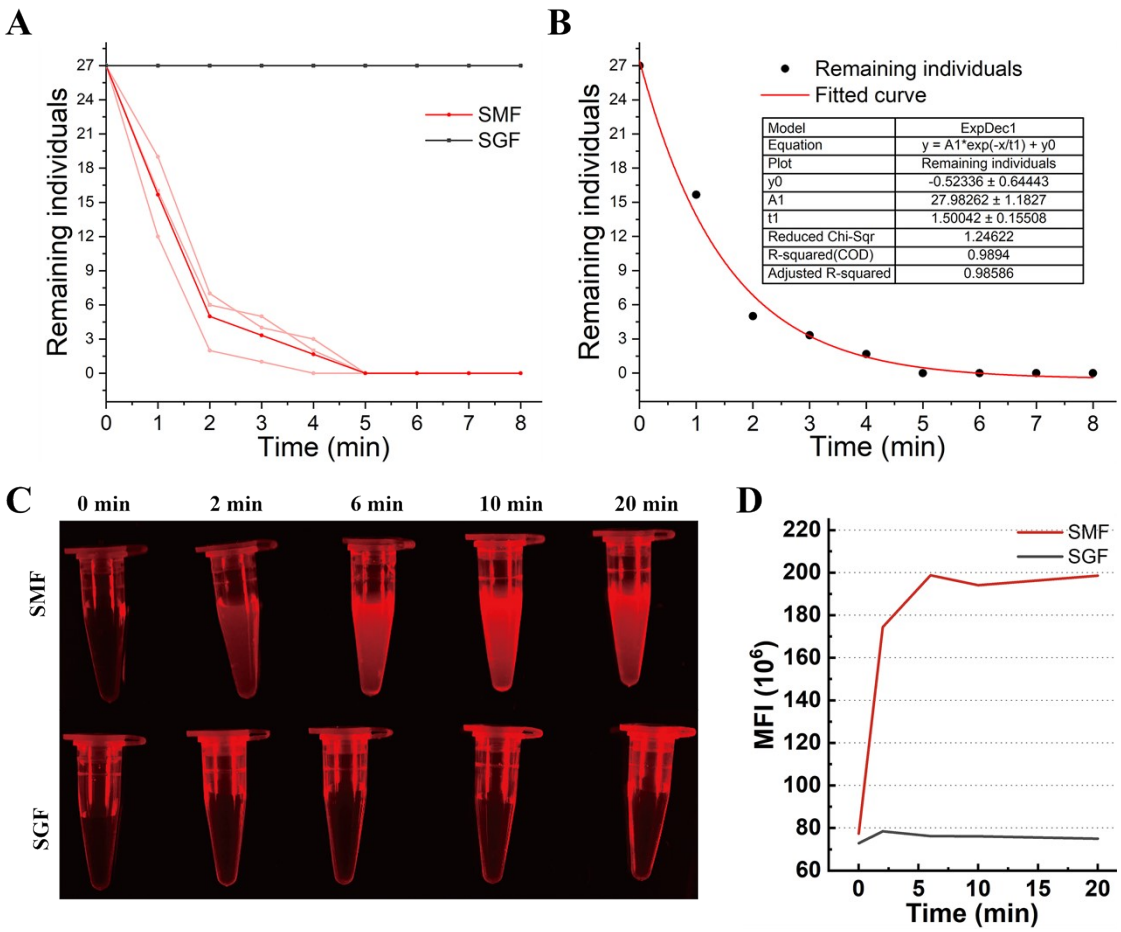

Figure S6. Different release behavior of the SMM in SMF or SGF. (A) The change in the number of remaining tips containers in SMF and SGF (n = 3). (B) The Fitted curve of the change in the number of remaining tips containers in SMF. (C) The fluorescence image of the mucosal-responsive release of the SMM in SMF and SGF. (D) The mean fluorescence intensity (MFI) curve of SMM in SMF and SGF.

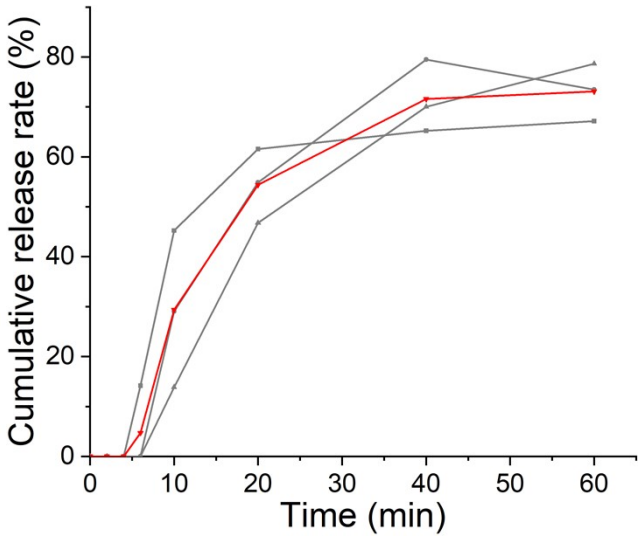

Figure S7. The cumulative release curve of insulin-loaded SMM (n = 3).

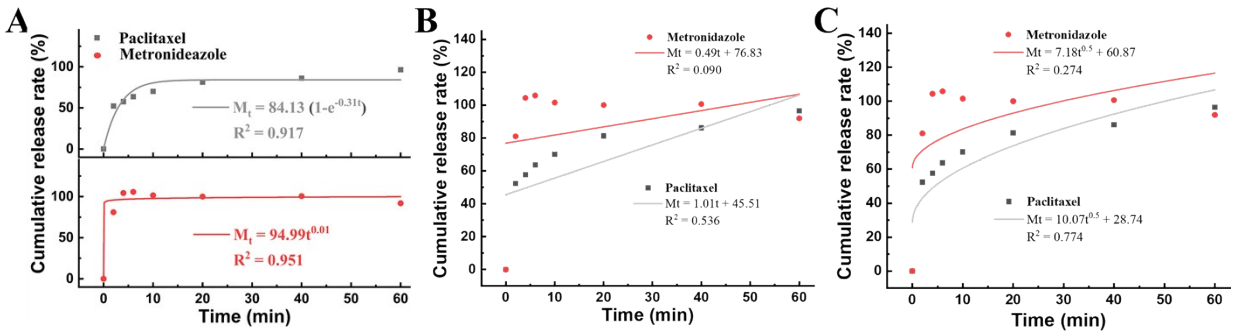

Figure S8. The other release fitting curves of SMM. (A)The first-order release fitting curves of SMM loaded with paclitaxel (upper) and the Korsmeyer–Peppas equation fitting curves of SMM loaded with metronidazole (lower). (B) The zero-order release fitting curve of SMM loaded with paclitaxel and metronidazole. (C) The Higuchi equation fitted curve of SMM loaded with paclitaxel and metronidazole.

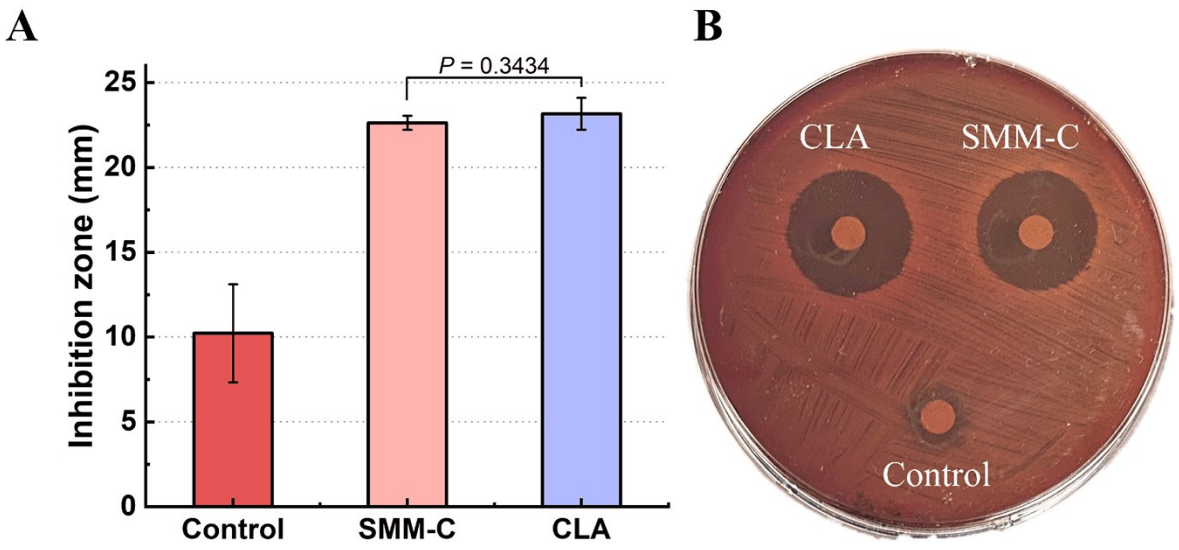

Figure S9. Inhibition zone test. (A) Inhibition zone of clarithromycin and SMM loaded with clarithromycin. Data were presented as mean ± SD (n = 3). (B) The photo of inhibition zone of clarithromycin and SMM loaded with clarithromycin.

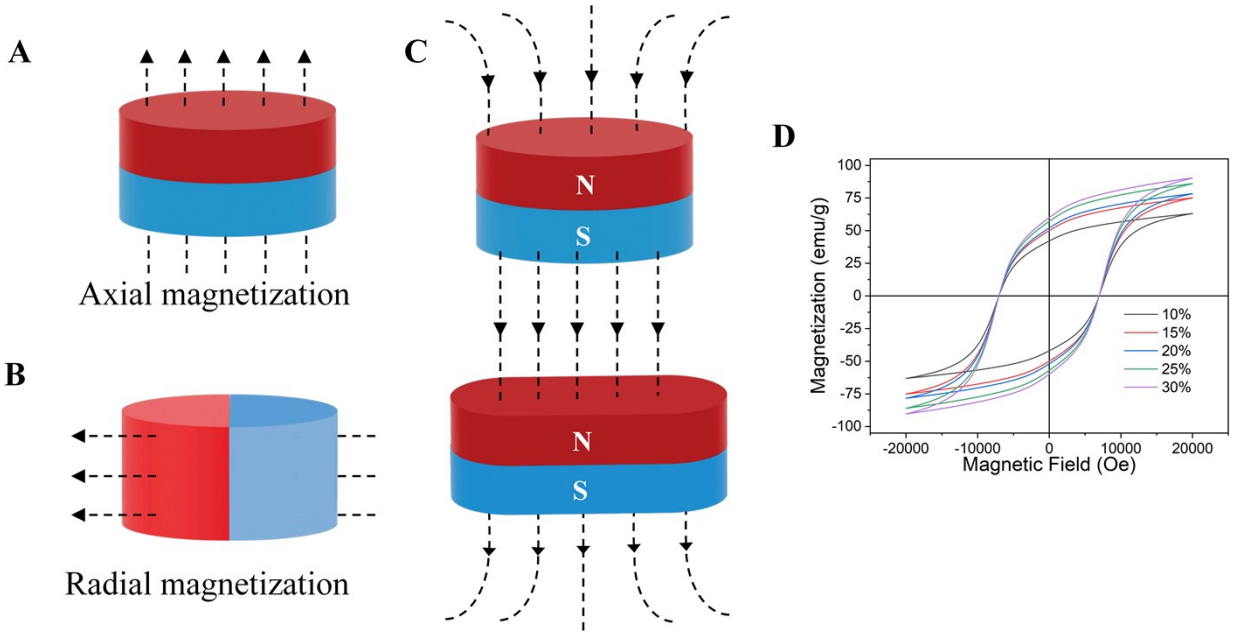

Figure S10. Schematic diagram of the magnetization direction and M-H curve of NdFeB-PCL base. (A) Axial magnetization. (B) Radial magnetization. (C) The interaction between the axial magnetized base and axial magnetized magnet. N indicated the north pole. S indicated the south pole. The dashed lines in (A - C) indicate the direction of the magnetic field. (D) M-H curve of NdFeB-PCL base with varying NdFeB contents (10 - 30%, w/v).

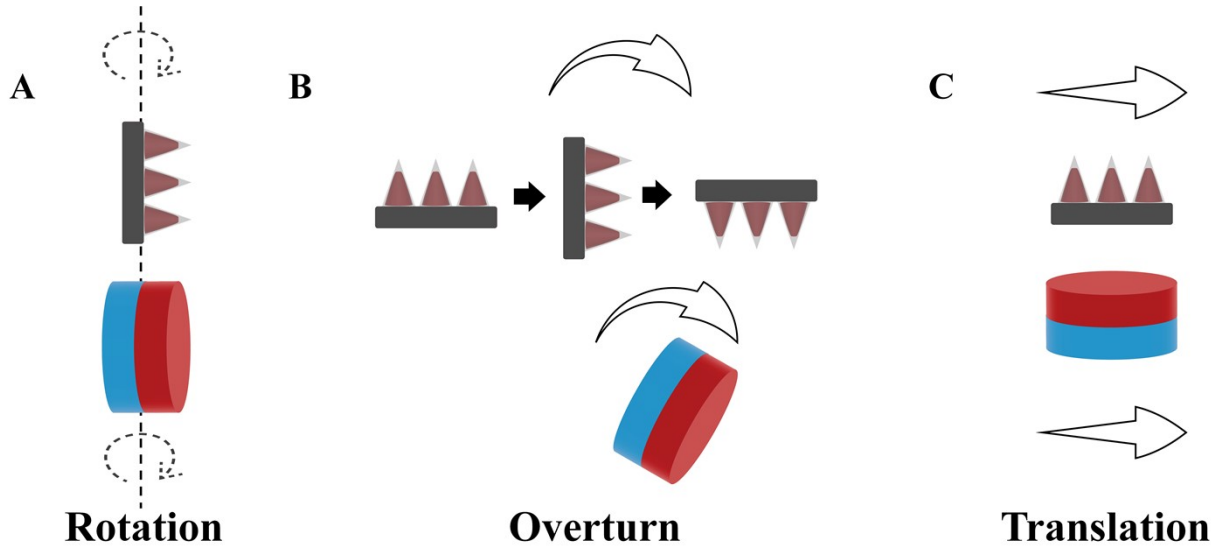

Figure S11. Schematic diagram of the interaction between magnet and SMM. (A) Rotational motion controlled by the magnet. (B) Overturning motion controlled by the magnet. (C) Translational motion controlled by the magnet.

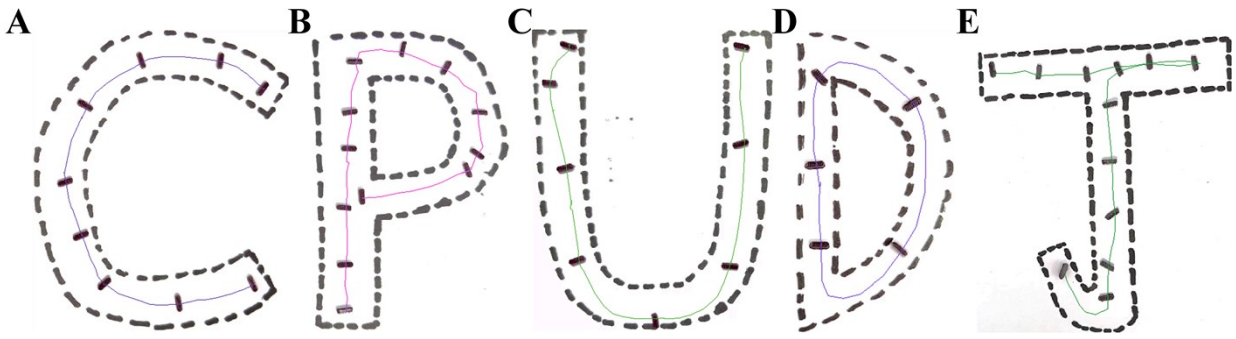

Figure S12. Alphabetical trajectory of SMM controlled by the external magnetic field. (A) The stroboscopic trajectory route of the SMM for translation along the shape of the letter C. (B) The stroboscopic image of SMM followed a trajectory route that flips along the shape of the letter P. (C) The stroboscopic trajectory route of the SMM for translation along the shape of the letter U. (D) The stroboscopic trajectory route of the SMM for translation along the shape of the letter D. (E) The stroboscopic image of SMM followed a trajectory route that flips along the shape of the letter J.

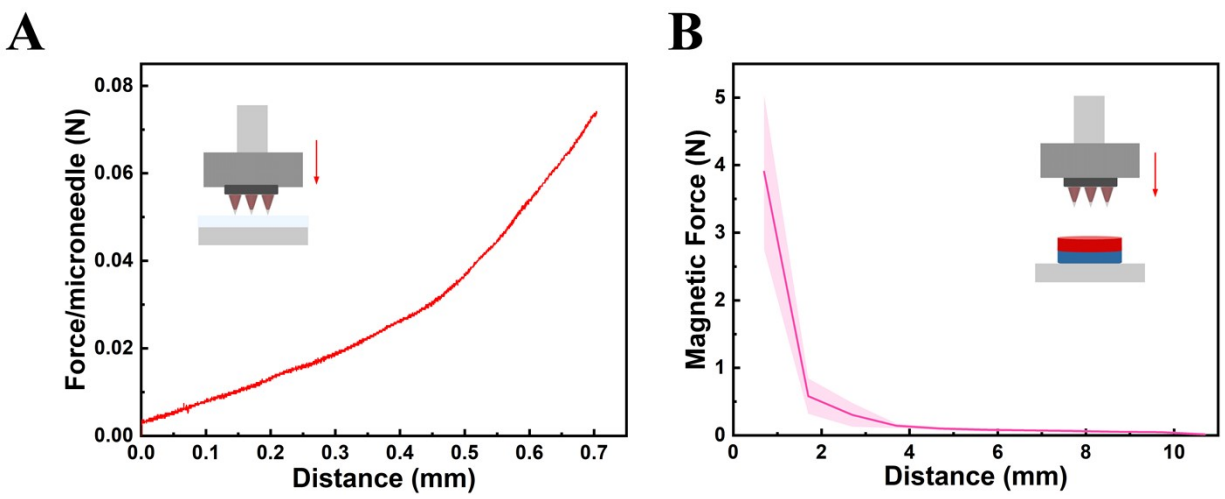

Figure S13. Analysis of the penetrating force and magnetic force. (A) Changes of the force per container as the SMM gradually penetrated into the 1% agarose hydrogel. The x-axis meant the distance between the fixed SMM and the agarose hydrogel. (B) Changes of the magnetic force generated by the approaching magnet. The x-axis meant the distance between the fixed SMM and the magnet. Data were presented as mean ± SD (n = 3).

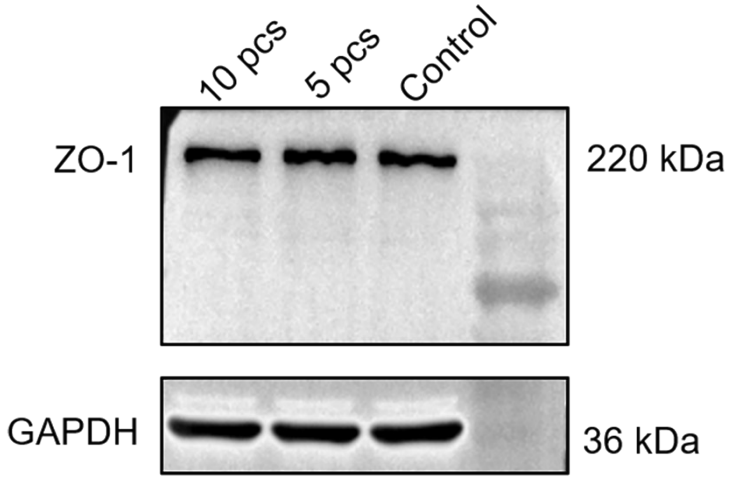

Figure S14. The effect of SMM on paracellular modulation. The impact of SMM on tight junction proteins ZO-1 expression level.

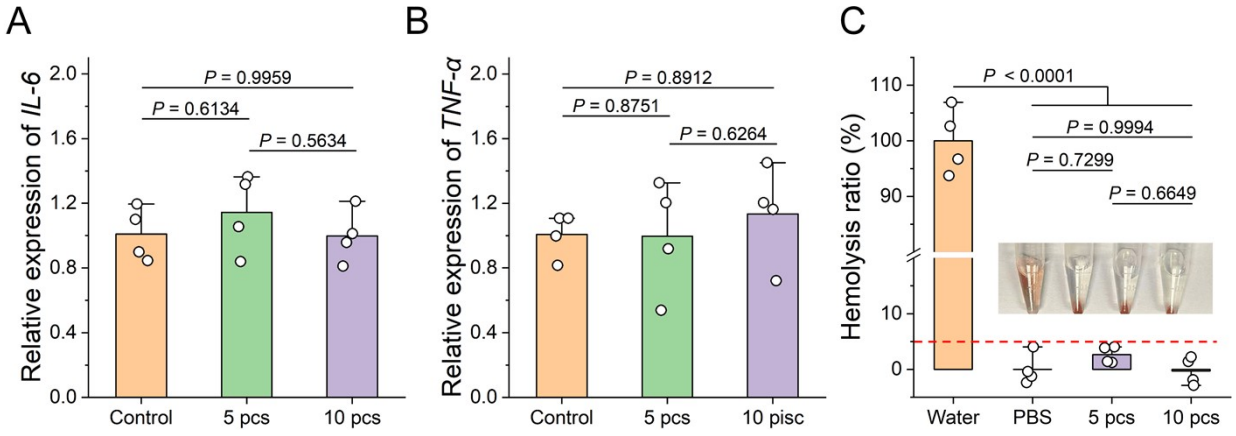

Figure S15. Immunogenicity and blood compatibility of SMM. IL-6 (A) and TNF-α (B) gene expression levels in macrophages following co-incubation with SMM (n = 4). (C) Hemolysis rates analysis of SMM. The red dotted line indicates the hemolysis rate threshold (n = 4).

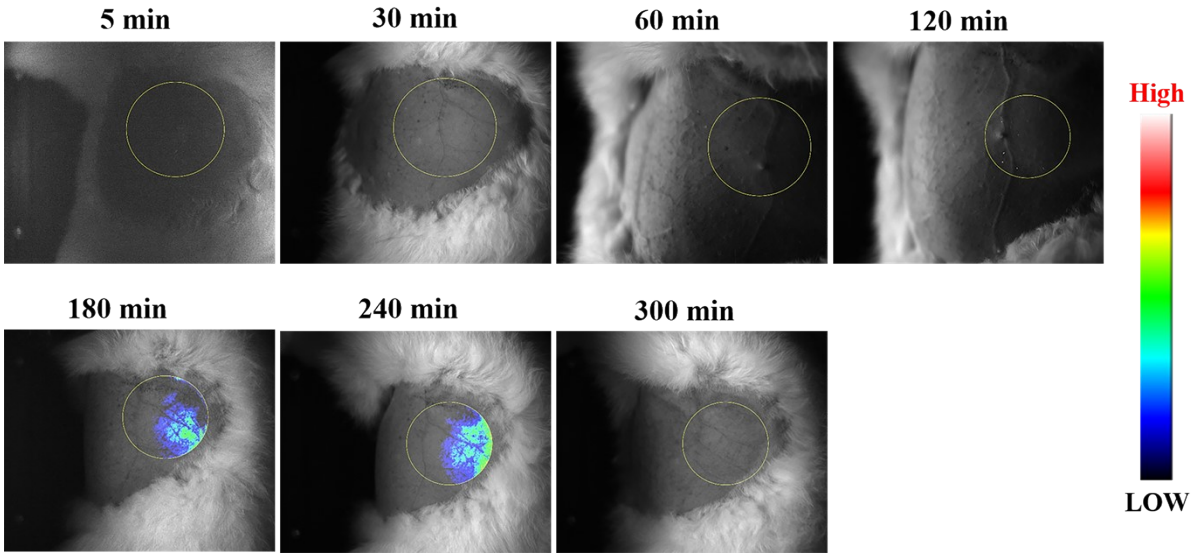

Figure S16. *In vivo* fluorescence imaging of rabbit. Fluorescence imaging of rabbit within 300 minutes after oral administration with 25-fold mass of R-B powders in solution form.

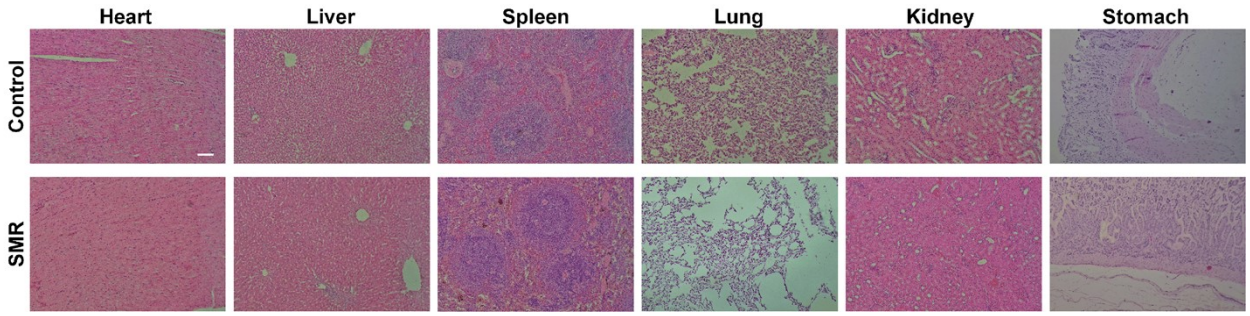

Figure S17. H&E staining of main organs of rabbits after SMM treatment. Scale bar: 100 μm.

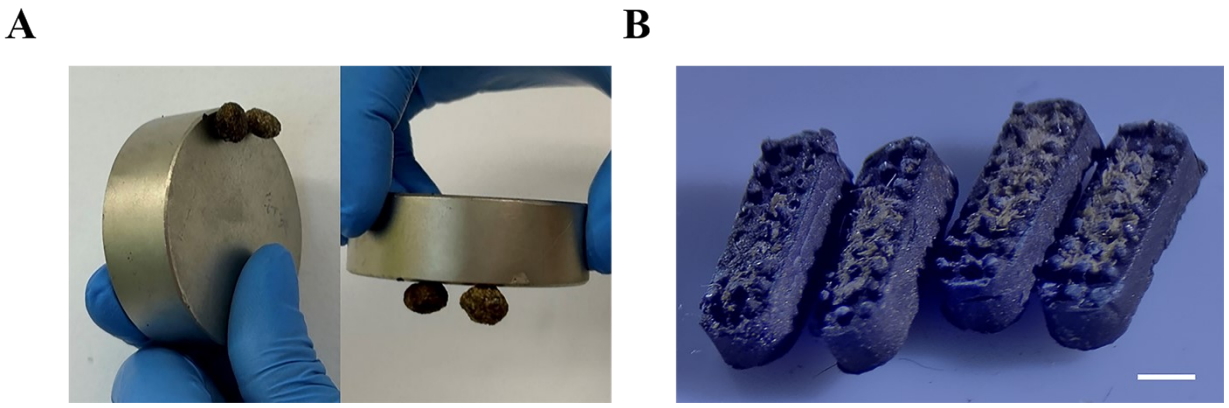

Figure S18. SMMs in rabbit feces. (A) Magnetic rabbit feces collected by the magnet. (B) The morphology of SMMs derived from rabbit feces. Scale bar:1000 μm.

Table 1. Primer Information Used in This Paper

Primer	Primer sequence
IL-6	F: AGTCCGGAGAGGAGACTTCA R: ATTTCCACGATTTCCCAGAG
TNF-α	F: ATGAGAAGTTCCCAAATGGC R: CTCCACTTGGTGGTTTGCTA
NAPDH	F: AGGTCGGTGTGAACGGATTTG R: GGGGTCGTTGATGGCAACA

Movie information

Video S1. Dynamic disintegration process of SMM in SMF and SGF.

Video S2. Rotation of SMM guided by a rotated magnet.

Video S3. Letter-shaped trajectory of the SMM directed by the magnet in plane.

Video S4. Enhanced retention of SMM navigated by the magnet under the impact of running water. Water speed is 99 mL min^{-1}.

Video S5. Climbing track of the SMM guided by the magnet in 3D-printed stomach model.

Video S6. Dynamic penetration and muco-responsive release of SMM navigated by the magnet on ex vivo rabbit stomach.

Video S7. The stomach wall traction caused by the attraction between SMM and the magnet in an isolated rat stomach.

Video S8. Dynamic process of SMM about magneto-responsive manipulation and penetration in dog stomach.

Video S9. Magnetic reactivity of rabbit feces containing the base.